Table 2
Image Noise in the Ascending Aorta and Right Ventricle

Variable	All Patients	Group A	Group B	Group C
No. of patients	428	145	145	138
SD (HU)				
Ascending aorta	17 ± 7 (11–30)	16 ± 3 (11–27)	17 ± 3 (11–30)	17 ± 2 (12–24)
Right ventricle	19 ± 4 (10–32)	19 ± 4 (10–32)	18 ± 4 (10–31)	20 ± 2 (16–26)
Mean + 2 SDs (HU)				
Ascending aorta	75 ± 9 (53–109)	75 ± 10 (53–99)	75 ± 10 (53–109)	76 ± 7 (57–100)

HU, Hounsfield units; SD, standard deviation.
Data are expressed as mean ± SD (range).

Figure 3. The highest standard deviation images in the three groups. Images with the highest noise in the three groups are shown. **(a)** An image of a 57-year-old woman (body mass index [BMI], 34.1 kg/m^2; body height, 155 cm) below the diaphragm level (SD = 32 Hounsfield units [HU]). **(b)** An image of a 57-year-old man (BMI, 27.1 kg/m^2; body height, 165 cm) was sacrificed to streaking artifact from spinal spur (SD = 31 HU). **(c)** An image of an 80-year-old man (BMI, 26.8 kg/m^2; body height, 164 cm) below the diaphragm shows pleural and pericardial effusion (SD = 26 HU).

$$\text{interobserver variability} = [\text{absolute}(\text{observer 1} - \text{observer 2})/(\text{observer 1} + \text{observer 2}) \times 0.5] \times 100,$$

where observer 1 and observer 2 are the CAC scores measured by the respective observers. Interscan variability, on a logarithmic scale, was compared among the three groups and CAC-scoring algorithms.

Radiation Dose

The dose-length product (in milligrays by centimeter) displayed on the dose report on the CT scanner was recorded. The effective dose was estimated by a method proposed by the European Working Group for Guidelines on Quality Criteria in Computed Tomography (16). In this method, the effective dose is derived from the dose-length product and a conversion coefficient for the chest (k = 0.017 mSv/mGy/cm averaged between male and female models). The effective doses in the three groups were plotted against BMI.

Statistical Analyses

All statistical analyses were performed using commercially available software package (MedCalc 9.5.1 for Windows; MedCalc Software, Mariakerke, Belgium). Categorical variables are presented as frequencies and percentages and continuous variables as mean ± SD. The χ^2 and analysis of variance (ANOVA; multivariate calculations)

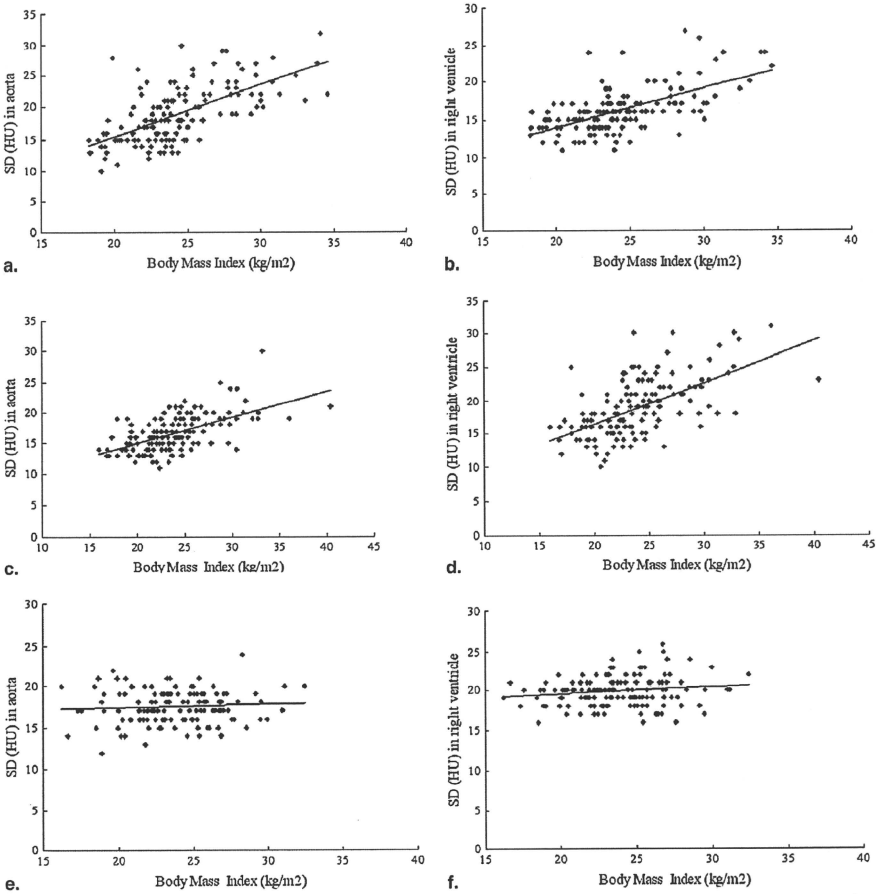

Figure 4. The relationship between standard deviation (SD) and body mass index (BMI). Scatterplots show the ratio between BMI (kg/m^2) and SD (Hounsfield units [HU]). **(a)** Group A, in the aorta: SD = 0.51 (95% confidence interval [CI], 0.40–0.62) × BMI + 4 ($P < .01$). **(b)** Group A, in the right ventricle: SD = 0.81 (95% CI, 0.64–0.97) × BMI − 1 ($P < .01$). **(c)** Group B, in the aorta: SD = 0.43 (95% CI, 0.33–0.53) × BMI + 6 ($P < .01$). **(d)** Group B, in the right ventricle: SD = 0.62 (95% CI, 0.48–0.76) × BMI + 4 ($P < .01$). **(e)** Group C, in the aorta: SD = 0.041 (95% CI, −0.069 to 0.15) × BMI + 16 ($P = .46$). **(f)** Group C, in the right ventricle: SD = 0.091 (95% CI, −0.013 to 0.20) × BMI + 18 ($P = .09$). The positive slopes of image noise versus BMI, 0.51 and 0.81 HU/(kg/m^2) in group A and 0.43 and 0.62 HU/(kg/m^2) in group B, suggest insufficient control of the tube current. In contrast, the nearly flat slopes of 0.041 and 0.091 HU/(kg/m^2) in group C indicate optimal control of tube current across patients.

Table 3
Coronary Artery Calcium Scores and Interscan and Interobserver Variability

Variable	All Patients	Group A	Group B	Group C
No. of patients	300	100	100	100
Agatston score				
Scan 1				
Observer 1	175 (48, 648)	206 (46, 664)	167 (42, 464)	152 (48, 775)
Observer 2	185 (48, 648)	206 (48, 668)	174 (42, 488)	157 (48, 789)
Scan 2				
Observer 1	179 (43, 610)	201 (46, 638)	171 (42, 444)	148 (39, 797)
Observer 2	176 (45, 611)	204 (46, 638)	176 (42, 462)	148 (39, 803)
Volume score				
Scan 1				
Observer 1	150 (43, 515)	165 (38, 548)	138 (39, 367)	125 (44, 639)
Observer 2	149 (43, 528)	166 (40, 552)	146 (37, 392)	129 (44, 622)
Scan 2				
Observer 1	144 (41, 502)	176 (39, 502)	144 (35, 356)	122 (41, 665)
Observer 2	146 (41, 502)	176 (40, 502)	146 (36, 366)	121 (41, 668)
Calcium mass				
Scan 1				
Observer 1	33 (8, 127)	37 (8, 130)	30 (7, 93)	28 (8, 139)
Observer 2	33 (8, 130)	37 (8, 132)	30 (7, 93)	28 (8, 139)
Scan 2				
Observer 1	32 (8, 123)	37 (8, 131)	30 (7, 89)	25 (7, 153)
Observer 2	32 (8, 123)	37 (8, 131)	30 (6, 91)	26 (7, 149)
Interscan variability (%)				
Agatston				
Observer 1	13, 8 (3, 17)	13, 7 (2, 15)	12, 6 (2, 15)	14, 10 (4, 18)
Observer 2	13, 8 (3, 17)	13, 7 (3, 16)	13, 6 (2, 16)	14, 10 (3, 20)
Volume				
Observer 1	12, 7 (3, 16)	12, 6 (3, 16)	11, 6 (2, 15)	11, 8 (3, 15)
Observer 2	11, 6 (3, 16)	11, 6 (2, 15)	10, 6 (2, 15)	12, 8 (3, 17)
Mass				
Observer 1	11, 6 (2, 14)	10, 4 (2, 14)	10, 5 (2, 11)	12, 8 (2, 14)
Observer 2	11, 6 (2, 14)	10, 4 (2, 14)	12, 5 (2, 11)	11, 8 (2, 14)
Interobserver variability (%)				
Agatston				
Scan 1	4, 1 (0, 3)	3, 1 (0, 4)	5, 0 (0, 3)	3, 0 (0, 2)
Scan 2	3, 0 (0, 3)	5, 0 (0, 3)	4, 0 (0, 2)	2, 1 (0, 1)
Volume				
Scan 1	2, 0 (0, 2)	3, 0 (0, 3)	3, 0 (0, 1)	1, 0 (0, 0)
Scan 2	2, 0 (0, 2)	3, 0 (0, 2)	4, 0 (0, 2)	1, 0 (0, 3)
Mass				
Scan 1	3, 1 (0, 1)	3, 0 (0, 2)	4, 0 (0, 2)	1, 0 (0, 1)
Scan 2	3, 0 (0, 1)	3, 0 (0, 2)	4, 0 (0, 1)	2, 0 (0, 1)

Coronary artery calcium is expressed as median (25th, 75th percentiles). Variability is expressed as mean, median (25th, 75th percentiles).

tests were used to determine group differences. P values $< .05$ were considered to identify significant differences.

RESULTS

All patients were able to hold their breath for the two scans. Baseline characteristics of the patients are presented in Table 1. Neither heart rate ($P = .47$) nor heart rate variation ($P = .44$) was different among the three groups. Three hundred of the overall 428 patients were CAC positive. One hundred twenty patients showing negative scores on both scans and eight patients showing both positive and negative scores between scans or between algorithms were excluded for the calculation of variability.

Table 4
Tube Current, Tube Current–Time Product, and Radiation Dose

Variable	All Patients	Group A	Group B	Group C	*P*
Tube current (mA)	227 ± 65 (75–610)	245 ± 36 (180–350)	227 ± 43 (150–370)	209 ± 94 (75–610)	<.01*
Tube current–time product (mAs)	53 ± 15 (18–142)	57 ± 8 (42–56)	53 ± 10 (35–86)	49 ± 25 (18–142)	<.01*
Dose0length product (mGy · cm)	49 ± 15 (16–131)	53 ± 8 (37–87)	49 ± 10 (30–84)	44 ± 21 (16–131)	<.01*
Estimate effective dose (mSv)	0.8 ± 0.3 (0.3–2.2)	0.9 ± 0.2 (0.6–1.5)	0.8 ± 0.2 (0.5–1.4)	0.8 ± 0.4 (0.3–2.2)	<.01*

Data are expressed as mean ± standard deviation (range).
* One-factor analysis of variance.

Image Noise

The SD and the mean + 2 SDs in regions of interest in the aorta and the right ventricle are presented in Table 2. The test for one mean revealed that the SD in the right ventricle was different from 20 HU in group A (95% confidence interval [CI], 18.3–19.7; $P < .01$) and group B (95% CI, 17.3–18.7; $P < .01$), whereas the SD was not different from 20 HU in group C (95% CI, 19.7–20.3; $P = 1.00$). In group C, the mean SD was 20 ± 2 HU (range, 16–26 HU). Images with the highest noise in the three groups are shown in Figure 3. In group C, six of 138 patients (4%) showed CT values > 23 HU in the right ventricle (at the maximal heart diameter level on the axial CT image). In five of the patients, the image levels were below the dome of the diaphragm, being different from the image used for the measurement of attenuation in the scout image.

The mean + 2 SDs did not exceed 130 HU in groups A and C, whereas the value in the right ventricle was 133 HU in one case in group B.

The regression analysis revealed a statistically significant influence of patient BMI on image noise in groups A and B (Figs 4a–d). In group C, however, nearly flat slopes of 0.04 and 0.091 HU/(kg/m^2) were seen between BMI and SD, indicating favorable control of tube current (Figs 4e and 4f).

CAC Scores and Interscan and Interobserver Variability

CAC scores and the interscan and interobserver variability are summarized in Table 3. The CAC scores were not different among the three groups. For a representative example, one-factor ANOVA revealed that there was no significant difference of log-transformed Agatston scores on scan 1 measured by observer 1 between the groups ($P = .61$). CAC scores were not different between scans and observers; for example, repeated-measures ANOVA revealed that there was no statistical significance of log-transformed Agatston scores in group A between the scans ($P = .31$) and observers ($P = .91$).

For observer 1, the mean interscan variability of CAC-positive patients in all groups ($n = 300$) was 13% (median, 8%) for Agatston score, 12% (median, 7%) for volume, and 11% (median, 6%) for mass. Two-factor ANOVA revealed that the interscan variability in CAC scores, on a logarithmic scale, was not different among the three groups ($P = .17$) and algorithms ($P = .07$).

Interobserver variability was small. For scan 1, the mean interobserver variability for Agatston score, volume, and mass in CAC-positive patients was 4% (median, 1%), 2% (median, 0%) and 3% (median, 1%), respectively.

Radiation Dose

The tube currents, tube current–time products, dose-length products, and estimated effective doses in the 3 groups are shown in Table 4. One-factor ANOVA revealed that there were significant differences in all values among the three groups ($P < .01$). Group C used the least dose and, more important, a wide range of doses (effective dose, 0.3–2.2 mSv). The plots of effective dose against BMI are shown in Figures 5a to 5c. In group C, the tube currents used and radiation doses were different among individuals and widely distributed compared with groups A and B.

DISCUSSION

The major points of the present study are as follows: (1) attenuation-based tube current control, at the level of the maximal heart diameter on the scout view, has the potential to favorably control image noise in CAC scoring; (2) low-dose scanning is possible, combined with prospective electrocardiographically triggered scanning; and (3) the protocol for 64-detector CT imaging provides low interscan and interobserver variability.

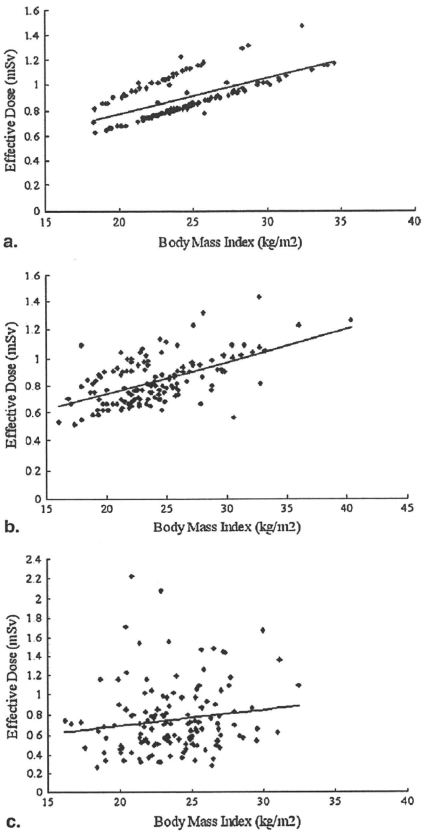

Figure 5. The relationship between effective dose and body mass index (BMI). Plots of effective dose against BMI are shown. **(a)** Group A: effective dose = 0.028 × BMI + 0.22 ($P < .01$). **(b)** Group B: effective dose = 0.023 × BMI + 0.27 ($P < .01$). **(c)** Group C: effective dose = 0.016 × BMI + 0.38 ($P = .11$). In groups A and B, effective dose was a function of BMI, but not in group C. The effective doses in group C were widely distributed, irrespective of BMI values.

Image Noise

In attenuation-based tube current control, the mean noise was controlled to the target value of 20 HU. In addition, the range was small compared to the BMI group and BMI and body height group. These facts indicate that attenuation-based scanning meets the goal of dose that is as low as reasonably achievable. Of the 138 patients in the attenuation-based group, the maximal mean + 2 SDs was 107 HU in the right ventricle. Because the CT value threshold of CAC detection was set to 130 HU, this result indicates that the noise is not likely to be falsely judged as CAC. This is also important because image noise is known to be one factor affecting interscan variability of CAC (17,18). In the BMI and BMI and body height groups, image noise was a function of BMI, suggesting insufficient control of the tube current in individual patients. Although an increase in body weight or BMI theoretically leads to an increase in image noise, the noise cannot be ideally controlled on the basis of these parameters.

Interscan and Interobserver Variability in CAC Scoring

The interscan variability of Agatston scores in 300 CAC-positive patients (for observer 1: mean, 13%; median, 8%) was lower than the variability on electron-beam CT imaging (20%–37%) (14,17,19,20) and was comparable to the variability on overlapping images from retrospective reconstruction on prior-generation (4-slice or 16-slice) multidetector CT imaging (21,22). The variability was also comparable to that on 64-detector CT imaging (23). However, the data on 64-detector CT imaging are from a single institution. It is our hope that more data from multiple institutions will be collected. Apart from overlapping images, the use of a volume or mass algorithm can further reduce variability. Although not significant ($P = .07$), this trend was observed in the present study, in line with previous studies (22,23). The interobserver variability in this study was small. Artificial lesions, known to affect interobserver variability, were reduced in the study, with favorably controlled noise. We consider the interscan and interobserver variability in the current study encouraging. However, prudence is called for in actual clinical practice, because patients are likely to have different heart rates when studies are performed a few years apart, and body habitus and position may also change, thus possibly increasing variability.

Radiation Dose

In the attenuation-based group, the tube currents and associated radiation doses were distributed over a wide range, and the doses were different even among patients with the same BMIs. This is considered an appropriate method in patients who do not require much dose (eg, slender patients who do not receive more dose than necessary). For example, the minimal dose was only 0.3 mSv for a small and slender patient (height, 151 cm; weight, 42 kg; BMI, 18 kg/m^2). We also found that the mean radiation dose in the attenuation-based group was the same as on electron-beam CT imaging (0.7 mSv) (24). We may therefore conclude that this level of

radiation dose may be suited for repeated examination to monitor the progression of atherosclerosis. Another approach for the reduction of dose is lowering the tube voltage (25,26). However, this requires need calibration for the calculation of a scanner with a specifically adapted threshold for the identification of calcium and is available only for calcium mass scoring.

A technical issue should be addressed. Because the current was determined at the maximal heart diameter on the scout view, image noise below the dome of the diaphragm tended to become higher. Indeed, five patients showed CT values > 23 HU in the right ventricle below the dome of the diaphragm. However, considering that the largest part of the coronary arteries was suggested to exist in the first 6 cm of the transverse scan (27), CAC below the diaphragmatic level is probably of less importance. Although we could have controlled the image noise by adjusting at such a lower level, we did not choose to do so, because it might have excessively increased radiation dose.

One limitation is that this study was conducted at a single institution in Japan, and the participants consisted of smaller patients than typical US citizens, resulting in a lower estimated dose than expected for US citizens. Nevertheless, the method is applicable to any patient and seems promising for the control of tube current in CAC scoring.

In conclusion, attenuation-based tube current control at the level of the maximal heart diameter on the scout view has the potential to favorably control image noise across patients. Low dose and low interscan variability on CAC scoring are shown on prospective electrocardiographically triggered 64-detector CT imaging.

REFERENCES

1. Greenland P, Bonow RO, Brundage BH, et al. ACCF/AHA 2007 clinical expert consensus document on coronary artery calcium scoring by computed tomography in global cardiovascular risk assessment and in evaluation of patients with chest pain. J Am Coll Cardiol 2007; 49: 378–402.
2. Takahashi N, Bae KT. Quantification of coronary artery calcium with multi-detector row CT: assessing interscan variability with different tube currents-pilot study. Radiology 2003; 228:101–106.
3. Shemesh J, Evron R, Koren-Morag N, et al. Coronary artery calcium measurement with multi-detector row CT and low radiation dose: comparison between 55 and 165 mAs. Radiology 2005; 236:810–814.
4. Mahnken AH, Wildberger JE, Simon J, et al. Detection of coronary calcifications: feasibility of dose reduction with a body weight-adapted examination protocol. AJR Am J Roentgenol 2003; 181:533–538.
5. Jung B, Mahnken AH, Stargardt A, et al. Individually weight-adapted examination protocol in retrospectively ECG-gated MSCT of the heart. Eur Radiol 2003; 13:2560–2566.
6. Horiguchi J, Yamamoto H, Hirai N, et al. Variability of repeated coronary artery calcium measurements on low-dose ECG-gated 16-MDCT. AJR Am J Roentgenol 2006; 187:W1–W6.
7. Sevrukov A, Pratap A, Doss C, Jelnin V, Hoff JA, Kondos GT. Electron beam tomography imaging of coronary calcium: the effect of body mass index on radiologic noise. J Comput Assist Tomogr 2002; 26:592–597.
8. Horiguchi J, Matsuura N, Yamamoto H, et al. Coronary artery calcium scoring on low-dose prospective electrocardiograph-triggered 64-slice CT. Acad Radiol 2009; 16:187–193.
9. McCollough CH, Ulzheimer S, Halliburton SS, et al. Coronary artery calcium: a multiinstitutional, multimanufacturer international standard for quantification at cardiac CT. Radiology 2007; 243:527–538.
10. Mühlenbruch G, Hohl C, Das M, et al. Evaluation of automated attenuation-based tube current adaptation for coronary calcium scoring in MDCT in a cohort of 262 patients. Eur Radiol 2007; 17:1850–1857.
11. Horiguchi J, Shen Y, Hirai N, et al. Timing on 16-slice scanner and implications for 64-slice cardiac CT: do you start scanning immediately after breath-hold? Acad Radiol 2006; 13:173–176.
12. Matsuura N, Horiguchi J, Yamamoto H, et al. Optimal cardiac phase for coronary artery calcium scoring on single-source 0.35 sec-rotation-speed 64-MDCT scanner—least interscan variability and least motion artifacts. AJR Am J Roentgenol 2008; 190:1561–1568.
13. Agatston AS, Janowitz WR, Hildner FJ, Zusmer NR, Viamonte M, Detrano R. Quantification of coronary calcium using ultrafast computed tomography. J Am Coll Cardiol 1990; 15:827–832.
14. Yoon HC, Greaser LE III, Mather R, Sinha S, McNitt-Gray MF, Goldin JG. Coronary artery calcium: alternate methods for accurate and reproducible quantitation. Acad Radiol 1997; 4:666–673.
15. Halliburton SS, Stillman AE, Lieber M, Kasper JM, Kuzmiak SA, White RD. Potential clinical impact of variability in the measurement of coronary artery calcification with sequential MDCT. AJR Am J Roentgenol 2005; 184:643–648.
16. Menzel H, Schibilla H, Teunen D. European guidelines for quality criteria for computed tomography. Brussels, Belgium: European Commission, 2000.
17. Achenbach S, Ropers D, Mohlenkamp S, et al. Variability of repeated coronary artery calcium measurements by electron beam tomography. Am J Cardiol 2001; 87:210–213.
18. Bielak LF, Kaufmann RB, Moll PP, MacCollough CH, Schwartz RS, Sheedy PF II. Small lesions in the heart identified at electron beam CT: calcification or noise? Radiology 1994; 192:631–636.
19. Callister TQ, Cooil B, Raya SP, et al. Coronary artery disease: improved reproducibility of calcium scoring with an electron-beam CT volumetric method. Radiology 1998; 208:807–814.
20. Wang SJ, Detrano BC, Secci A, et al. Detection of coronary calcification with electron-beam computed tomography: evaluation of interexamination reproducibility and comparison of three image-acquisition protocols. Am Heart J 1996; 132:550–558.
21. Ohnesorge B, Flohr T, Fischbach R, et al. Reproducibility of coronary calcium quantification in repeat examinations with retrospectively ECG-gated multisection spiral CT. Eur Radiol 2002; 12:1532–1540.
22. Horiguchi J, Yamamoto H, Akiyama Y, et al. Variability of repeated coronary artery calcium measurements by 16-MDCT with retrospective reconstruction. AJR Am J Roentgenol 2005; 184:1917–1923.
23. Horiguchi J, Matsuura N, Yamamoto H, et al. Variability of repeated coronary artery calcium measurements by 1.25-mm- and 2.5-mm-thickness images on prospective electrocardiograph-triggered 64-slice CT. Eur Radiol 2008; 18:209–216.
24. Morin RL, Gerber TC, McCollough CH. Radiation dose in computed tomography of the heart. Circulation 2003; 107:917–922.
25. Thomas CK, Mühlenbruch G, Wildberger JE, et al. Coronary artery calcium scoring with multislice computed tomography. in vitro assessment of a low tube voltage protocol. Invest Radiol 2006; 41:668–673.
26. Jakobs TF, Wintersperger BJ, Herzog P, et al. Ultra-low-dose coronary artery calcium screening using multislice CT with retrospective ECG gating. Eur Radiol 2003; 13:1923–1930.
27. Vliegenthart R, Song B, Hofman A, Witteman JCM, Oudkerk M. Coronary calcification at electron-beam CT: effect of section thickness on calcium scoring in vitro and in vivo Radiology 2003; 229:520–525.

International Journal of Cardiology xxx (2011) xxx–xxx

Contents lists available at ScienceDirect

International Journal of Cardiology

journal homepage: www.elsevier.com/locate/ijcard

Association between epicardial adipose tissue volume and characteristics of non-calcified plaques assessed by coronary computed tomographic angiography

Toshiharu Oka [a], Hideya Yamamoto [a,*], Norihiko Ohashi [a], Toshiro Kitagawa [a], Eiji Kunita [a], Hiroto Utsunomiya [a], Ryo Yamazato [a], Yoji Urabe [a], Jun Horiguchi [b], Kazuo Awai [c], Yasuki Kihara [a]

[a] Department of Cardiovascular Medicine, Hiroshima University, Graduate School of Biomedical Sciences, Hiroshima, Japan
[b] Department of Clinical Radiology, Hiroshima University Hospital, Hiroshima, Japan
[c] Department of Diagnostic Radiology, Hiroshima University, Graduate School of Biomedical Sciences, Hiroshima, Japan

ARTICLE INFO

Article history:
Received 11 December 2010
Received in revised form 1 April 2011
Accepted 24 April 2011
Available online xxxx

Keywords:
Cardiac computed tomography
Epicardial adipose tissue
Low-density plaque
Positive remodeling

ABSTRACT

Background: The aim of this study was to investigate whether high epicardial adipose tissue (EAT) volume is related to the presence of vulnerable coronary plaque components as assessed by computed tomography (CT).

Methods: We evaluated 357 patients referred for 64-slice CT, and assessed coronary plaque components and EAT volume. Vulnerable coronary plaque components were defined as the presence of non-calcified plaque (NCP), including low-density plaque (LDP: <39 HU) and positive remodeling (PR: remodeling index >1.05). In accordance with a previous report, patients were assigned to two groups: low (<100 ml) or high (≥100 ml) EAT volume.

Results: Compared to the low EAT volume group, the high EAT volume group had a higher prevalence of NCP (74% vs. 59%, $p=0.003$). Additionally, the high EAT volume group had a higher prevalence of LDP with PR than the low EAT volume group (46% vs. 25%, $p<0.001$). Interestingly, a high EAT volume was an independent predictor of LDP with PR (odds ratio 2.56, 95% confidence interval 1.38–4.85, $p=0.003$) after adjusting for age, gender, traditional cardiovascular risk factors, body mass index (BMI), abdominal visceral adipose tissue (VAT), and coronary artery calcium (CAC) scores.

Conclusions: A high EAT volume was associated with the presence of vulnerable plaque components, independent of obesity measurements (BMI and VAT) and CAC scores.

1. Introduction

Several studies have demonstrated that excessive fat accumulation in abdominal viscera is associated with coronary artery disease (CAD), myocardial infarction, and cardiovascular mortality [1, 2]. In our previous studies using computed tomography (CT), abdominal visceral adipose tissue (VAT) was a critical and independent determinant for, not only the presence, but also the extent of coronary artery calcium (CAC) scores [3]. This was also a determinant for non-calcified coronary plaques (NCPs) [4]. It has been reported that both epicardial and abdominal adipocytes are derived from the splanchnopleuric mesoderm, and that adipokines derived from the epicardial adipose tissue (EAT) surrounding coronary arteries may directly affect vessel walls, as well as the progress of atherosclerosis [5].

Recent advances in cardiac CT technology have enabled the identification and characterization of NCPs. Plaque components and vascular remodeling can be reliably assessed by 64-slice CT angiography, and NCPs with low CT density and positive remodeling (PR) frequently co-exist in potentially vulnerable lesions [6-8]. Although several studies have suggested that EAT is associated with CAC scores and coronary artery disease [9, 10], the association between EAT and NCPs remains unclear. The aim of the present study was to investigate the relationships between EAT volume and the presence of NCP vulnerable components, as defined by CT angiography.

2. Methods

2.1. Subjects

Between December 2007 and April 2009, a total of 495 consecutive patients with suspected CAD underwent a 64-slice CT assessment at our institution. For the present study, we excluded 138 subjects with a history of coronary revascularization ($n=110$), inadequate image quality because of motion artifacts or inadequate contrast concentration ($n=18$), or with missing information for one or more traditional CAD risk factors ($n=10$). Eventually, 357 patients were included in this study. In all patients, plain cardiac and abdominal scans were performed to measure the CAC scores

* Corresponding author at: Department of Cardiovascular Medicine, Hiroshima University, Graduate School of Biomedical Sciences, 1-2-3 Kasumi Minami-ku, Hiroshima 734-8551, Japan. Tel.: +81 82 257 5540; fax: +81 82 257 1569.
E-mail address: hideyayama@hiroshima-u.ac.jp (H. Yamamoto).

0167-5273/$ – see front matter
doi:10.1016/j.ijcard.2011.04.021

Please cite this article as: Oka T, et al, Association between epicardial adipose tissue volume and characteristics of non-calcified plaques assessed by coronary computed tomographic angiography, Int J Cardiol (2011), doi:10.1016/j.ijcard.2011.04.021

and the VAT areas. The study protocol was approved by the Ethical Committee at Hiroshima University, and written informed consent was obtained from all patients.

2.2. Risk factor assessments

All patients provided detailed clinical information at their clinical consultation. Hypertension was defined as a patient systolic blood pressure ≥ 140 mmHg, a diastolic blood pressure ≥ 90 mmHg, or the current use of antihypertensive medications. Hypercholesterolemia was defined as a low-density lipoprotein (LDL) cholesterol level ≥ 140 mg/dl on direct measurement, a total cholesterol level ≥ 220 mg/dl, or the current use of lipid-lowering drugs. Diabetes mellitus (DM) was defined by self-reporting, a glycohemoglobin A1c (HbA1c) level ≥ 6.5% [11], or the current use of hypoglycemic agents. Patients who smoked regularly during the previous year were classified as current smokers.

2.3. CT angiography and image analysis

CT examinations were performed using a 64-slice CT scanner (LightSpeed VCT, GE Healthcare, Waukesha, Wisconsin, USA). Patients orally received 40 mg metoprolol 60 min before CT scanning if the patient's resting heart rate was >60 beats/min; all patients received 0.3 mg nitroglycerin just before scanning. Prior to CTA, 35–40 contiguous images were obtained with a 2.5-mm slice thickness to measure the CAC scores, according to the Agatston method [12]. Contrast-enhanced scanning, and the scan protocol and reconstruction methods, were performed, as previously described [6, 7]. The effective radiation dose was estimated based on the dose-length product, and ranged from 15 to 18 mSv. Image reconstruction was performed using the CardIQ image analysis software program (GE Healthcare) on a dedicated computer workstation (Advantage Workstation Ver.4.2, GE Healthcare).

2.4. Plaque characterization

All coronary segments >2 mm in diameter were evaluated by two experienced independent observers using curved multi-planar reconstructions and cross-sectional images rendered perpendicularly to the vessel center line. CAD was defined by a cross-sectional narrowing >50% in epicardial coronary arteries.

Atherosclerotic plaques were classified as calcified or non-calcified. Calcified plaques were defined as lesions composed exclusively of structures with a CT density greater than that of the contrast-enhanced coronary lumen, or with a CT density >130 HU assigned to the coronary artery wall in a plain image. NCPs were defined as a low-density mass >1 mm^2 in size located within the vessel wall and clearly distinguishable from the contrast-enhanced coronary lumen and the surrounding pericardial tissue. In regard to the extent of calcified plaque and NCP, a high plaque count was defined as ≥ 2, and a low plaque count as ≤ 1. We further evaluated the NCP components by determining the minimal CT density, the vascular remodeling index (RI), and adjacent coronary calcium, as previously described [6, 7]. Briefly, the minimum CT density was determined to be the lowest average value of at least five regions of interest (area = 1 mm^2). A low-density plaque (LDP) was defined as a lesion with a minimum CT density <39 HU [6, 7]. Vascular remodeling was assessed using the RI, which was calculated by dividing the cross-sectional lesion vessel area by the proximal reference vessel area. Positive remodeling (PR) was defined as a RI > 1.05 [6, 7]. Spotty calcium was defined as calcium burden length < 3/2 of the vessel diameter and a width < 2/3 of the vessel diameter.

2.5. Measurement of VAT area and EAT volume using CT

Abdominal scans were performed at the 4th and 5th lumbar levels in the spinal position. The VAT area was defined as the intraperitoneal adipose tissue area at the level of umbilicus using commercial software (Virtual Place, AZE INC., Tokyo, Japan) [3, 4].

Using cross-sectional CT images for calcium scoring, EAT was defined as the adipose tissue between the epicardial surface of the myocardium and the pericardium. The EAT area within the manually traced epicardium was defined as having a density range between −250 and −30 HU and was automatically quantified using the same software as for the VAT area. EAT volume was calculated as the total sum of the EAT areas from the atrial appendage (i.e. 1 cm above the left main coronary artery) to the apex with 1 cm thick spacing between each image, as was previously described [10]. Based on the findings of Sarin et al. [10], a cut-off value of 100 ml for EAT volume was used, and patients were assigned to two groups, either the low (<100 ml) or the high (≥ 100 ml) EAT volume group. Intra- and inter-observer variability for the quantification of EAT volumes were calculated by the formula as previously reported [13].

2.6. Statistical analysis

Categorical variables are presented as the numbers of patients (percentage), and continuous variables are expressed as means ± SD or medians (interquartile range). For each variable, differences were evaluated using the Pearson χ^2-tests for categorical variables and the Student t test or the Mann–Whitney U test for continuous variables. We then assessed whether the associations between high EAT volume and the presence of NCP components were independent of age, gender, traditional coronary risk factors, BMI, VAT area, and CAC scores via multivariate logistic regression analyses. All analyses were performed using the JMP 8.0.2 software program (SAS Institute, Tokyo, Japan). P values < 0.05 were considered to be statistically significant.

3. Results

3.1. Patient characteristics and EAT volume measurement

The mean age of the study population was 66 ± 11 years old, and 64% of the subjects were male. The prevalence of coronary risk factors was as follows: hypertension (68%), hypercholesterolemia (50%), DM (31%), and smoking (31%). The mean BMI was 24.2 ± 4.8 kg/m^2. A total of 124 patients (35%) had CAD. The mean EAT volume was 125 ± 44 ml.

Baseline clinical characteristics and CT quantification are listed in Table 1. The high EAT volume group had higher BMIs, VAT areas, percentage of patients who were current smokers, and proportion of individuals with DM compared to the low EAT volume group. The prevalence of patients with CAD and a CAC score > 0 was higher in the high EAT volume group than in the low EAT volume group (38% vs. 26%, $p = 0.026$, 78% vs. 64%, $p = 0.005$, respectively). In comparison to the low EAT volume group, the high EAT volume group had a higher prevalence and extent (≥ 2 counts) of calcified plaques (70% vs. 58%, $p = 0.027$, and 54% vs. 41%, $p = 0.026$, respectively) and NCPs (74% vs. 59%, $p = 0.003$, and 52% vs. 40%, $p = 0.041$, respectively). Fig. 1 shows the comparison of NCP with vulnerable plaque components in patients with low vs. high EAT volume. The high EAT volume group had a higher prevalence of LDP (52% vs. 27%, $p < 0.001$), PR (58% vs. 37%, $p < 0.001$), and LDP with PR (46% vs. 25%, $p < 0.001$) compared to the low EAT volume group. Intra- and inter-observer variability for the quantification of EAT volumes were 3.0% and 4.8%, respectively.

3.2. Relationship between high EAT volume and the presence of NCP vulnerable components

Table 2 shows the results of age and sex-adjusted and multivariate analyses of the relationships between high EAT volume and NCP components. After adjusting for age, gender, hypertension, DM, smoking, BMI, and VAT area, Model-1 shows that high EAT volume

Table 1
Baseline characteristics and CT findings in patients with low and high EAT volume ($n = 357$).

Characteristics	Low EAT volume (<100 ml)	High EAT volume (≥100 ml)	p value
	$n = 107$	$n = 250$	
Age (years)	64.2 ± 11.1	66.3 ± 10.7	0.090
Male gender	63 (59)	165 (66)	0.199
Body mass index (kg/m^2)	22.0 ± 2.9	25.1 ± 5.2	<0.001
Hypercholesterolemia	50 (47)	128 (51)	0.44
Family history	17 (17)	37 (16)	0.79
Current smoker	24 (22)	86 (34)	0.025
Hypertension	66 (62)	176 (70)	0.11
Diabetes mellitus	21 (20)	90 (36)	0.002
Total cholesterol (mg/dl)	199.1 ± 38.1	201.3 ± 35.9	0.60
Triglyceride (mg/dl)	137.5 ± 100.8	154.7 ± 86.1	0.10
LDL cholesterol (mg/dl)	115.3 ± 32.4	120.7 ± 29.7	0.13
HDL cholesterol (mg/dl)	62.6 ± 18.1	58.0 ± 17.9	0.026
HbA1c (%)	5.71 ± 1.24	5.98 ± 1.01	0.029
VAT area (cm^2)	74.9 ± 35.1	120.6 ± 45.6	<0.001
Coronary artery disease	28 (26)	96 (38)	0.026
CAC scores	46 (0–236)	54 (0–242)	0.50
CAC scores > 0	68 (64)	194 (78)	0.005
Calcified plaque	62 (58)	175 (70)	0.027
Calcified plaque counts ≥ 2	44 (41)	135 (54)	0.026
Non-calcified plaque	63 (59)	186 (74)	0.003
Non-calcified plaque counts ≥ 2	43 (40)	130 (52)	0.041

Values are expressed as number (percent), mean ± SD, or median (interquartile range).
LDL: low-density lipoprotein; HDL: high-density lipoprotein; HbA1c: glycohemoglobin A1c; VAT: visceral adipose tissue; CAC: coronary artery calcium.

Please cite this article as: Oka T, et al, Association between epicardial adipose tissue volume and characteristics of non-calcified plaques assessed by coronary computed tomographic angiography, Int J Cardiol (2011), doi:10.1016/j.ijcard.2011.04.021

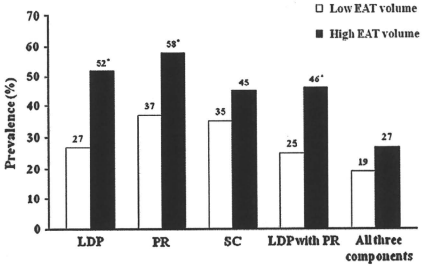

Fig. 1. Comparison of vulnerable plaque components in patients with low vs. high EAT volume.LDP: low-density plaque; PR: positive remodeling; SC: spotty calcium.* $p<0.05$ vs. low EAT volume group.

was independently associated with the presence of LDP (OR 2.90, 95% CI 1.59–5.42, $p<0.001$), PR (OR 1.94, 95% CI 1.07–3.54, $p=0.030$), and LDP with PR (OR 2.42, 95% CI 1.32–4.51, $p=0.005$). After adjusting for the variables in Model-1, as well as CAC scores, Model-2 shows that high EAT volume was still an independent predictor for the presence of LDP (OR 3.08, 95% CI 1.66–5.83, $p<0.001$), PR (OR 2.08, 95% CI 1.12–3.88, $p=0.021$), and LDP with PR (OR 2.56, 95% CI 1.38–4.85, $p=0.003$). Fig. 2 shows a representative case with high EAT volume presenting vulnerable plaque components.

4. Discussion

The present study demonstrates the relationships between coronary NCP components and EAT volume as measured by CT. The data indicate that a high accumulation of EAT is associated with the existence of NCP components (considered to be rupture-prone vulnerable features of plaque) after adjustment for other obesity measurements (BMI and VAT area) and CAC scores. The EAT measurement may provide novel and additional risk stratification for patients suspected of coronary artery disease.

4.1. EAT measurement

In the present study, we have demonstrated that EAT volume by CT is noninvasively measured and had a high reproducibility. Recently, several studies have shown that cardiac CT scans and magnetic resonance imaging can quantify EAT volume with high reproducibility, and are thereby effective tools for measuring EAT volume [10, 13-16]. In our CT study, using plane axial slices for calcium scoring, patients could obtain additional clinical information of risk stratification without additional radiation exposure or cost.

Our methods of measuring EAT volume can be utilized to evaluate the amount of adipose tissue surrounding coronary arteries. Using an EAT volume cut-off of 100 ml, which was based on the findings of Sarin et al. [10], we were able to detect LDP with PR at a sensitivity of 80%, a specificity of 41%, and an accuracy of 57%. Thus, the EAT volume cut-off of 100 ml is highly sensitivity, and can be used as a screening tool for detecting NCP with vulnerable coronary plaque components.

On the other hand, an echocardiographic study has shown the relationship between EAT thickness and coronary atherosclerosis [17]. Saura et al. [18] showed that EAT thickness measured by echocardiography had a poor reproducibility. Although transthoracic echocardiography is a simple and easy method to assess EAT volume, it is difficult to distinguish between small amounts of EAT and pericardial effusion and to measure EAT accurately in obese patients due to their poor echo images.

4.2. The relationship between EAT and coronary atherosclerosis

We revealed that high EAT volume was associated with not only the presence of CAD but also that of vulnerable plaque components. Several previous studies have demonstrated that high EAT volume was related to the existence of CAD [10] or myocardial ischemia as assessed by single photon emission computed tomography [19]. According to these findings, the accumulation of EAT around coronary arteries may contribute to the development of coronary atherosclerosis.

Several studies have reported the relationships between EAT volume and coronary plaque components. Konishi et al. [13] showed that high EAT volume was independently and significantly associated with the presence of coronary plaques, especially non-stenotic and non-calcified plaques using 64-slice CT. Alexopoulos et al. [20] have demonstrated that EAT volume was greater in patients with mixed and non-calcified plaques than in patients without plaques. In the present study, we assessed more detailed plaque components of coronary plaques than previous studies. Interestingly, we clarified that a high EAT volume was associated with the presence of LDP with PR. We found clinical significance when evaluating the EAT volume to predict patients at a high risk for vulnerable plaque components, which may contribute to acute coronary syndrome [6-8]. In a sub-analysis of the Multi-Ethnic Study of Atherosclerosis, a high pericardial adipose tissue volume was also associated with future incident coronary heart disease [21], which is consistent with our results.

Notably, our results revealed that higher EAT volumes are associated with the presence of LDP with PR after adjusting for BMI and VAT area. It was reported that the EAT thickness was associated with an increasing number of CAD lesions after adjusting for conventional risk factors, BMI, and VAT [16]. Consistent with our results, several reports have shown that EAT accumulation is associated with CAD and CAC scores in non-obese patients [22, 23]. Further, our results suggest that a high EAT volume is an independent predictor for vulnerable plaque components even after adjusting for CAC scores. Thus, EAT volume measurements, along with CAC scores, could be used to predict whether a patient is at high risk for vulnerable plaque components. The local effect of EAT on coronary arteries may play an important role in plaque formation. It can be speculated that a high EAT volume may be a direct and intimate

Table 2
Relationship between high epicardial adipose tissue volume and non-calcified plaque components.

Plaque components	Age and sex-adjusted		Multivariate (Model-1)[a]		Multivariate (Model-2)[b]	
	OR (95% CI)	p value	OR (95% CI)	p value	OR (95% CI)	p value
Low-density plaque	2.66 (1.60–4.49)	<0.001	2.90 (1.59–5.42)	<0.001	3.08 (1.66–5.83)	<0.001
Positive remodeling	2.08 (1.28–3.42)	0.004	1.94 (1.07–3.54)	0.030	2.08 (1.12–3.88)	0.021
Spotty calcium	1.34 (0.82–2.23)	0.25	1.08 (0.59–1.97)	0.80	1.11 (0.61–2.04)	0.73
Low-density plaque with positive remodeling	2.36 (1.42–4.02)	0.001	2.42 (1.32–4.51)	0.005	2.56 (1.38–4.85)	0.003
All three characteristics	1.42 (0.80–2.58)	0.24	1.49 (0.75–3.02)	0.26	1.65 (0.81–3.44)	0.17

OR: odds ratio; CI: confidence interval.
[a] Adjusted for age, sex, hypertension, hypercholesterolemia, diabetes mellitus, current smoking, body mass index, and visceral adipose tissue area.
[b] Adjusted for variables in Model-1 and CAC scores.

Please cite this article as: Oka T, et al, Association between epicardial adipose tissue volume and characteristics of non-calcified plaques assessed by coronary computed tomographic angiography, Int J Cardiol (2011), doi:10.1016/j.ijcard.2011.04.021

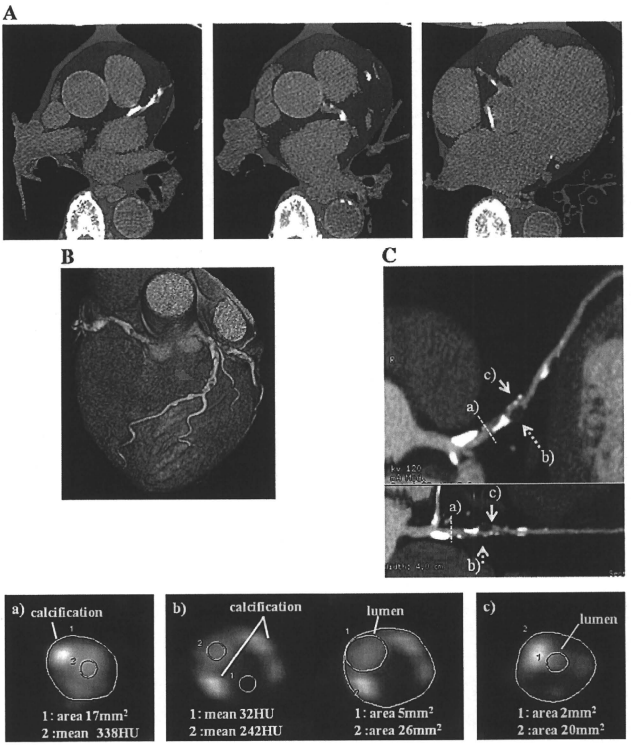

Fig. 2. A representative case with high accumulation of EAT presenting coronary atherosclerotic plaque with vulnerable plaque components.A density range between −250 and −30 HU was assigned as the adipose tissue. The EAT area (blue area) was manually traced on the epicardium (panel A). In this case, the EAT volume was 216 ml. The volume rendering image shows an atherosclerotic lesion in the middle portion of the left anterior descending artery (LAD) (panel B, blue arrow). The multi-planar reconstruction image of LAD shows an obstructive non-calcified plaque lesion with low-density plaque, positive vascular remodeling, and adjacent spotty calcium (panel C). The remodeling index is 1.53, calculated from the cross-sectional images of the reference site (a) and the lesion site (b). The minimum CT density of the lesion site is 32 HU. Adjacent spotty calcium can be observed in the cross-sectional image (a,b, and c).

source of adipokines, and thereby abnormal adipokine signaling in and around the coronary arteries. As in our previous report [4], high VAT area is significantly associated with NCP vulnerable components. We believe that VAT and EAT may work synergistically to accelerate coronary atherosclerosis and plaque vulnerability from inside and from outside the vessel walls, respectively.

4.3. Limitations

In the present study, we could not measure serum or tissue inflammatory cytokines and adipokines, both of which can lead to accelerate atherosclerosis or plaque vulnerability. A previous study demonstrated that the EAT in patients with critical CAD had a higher expression level of inflammatory mediators compared with subcutaneous adipose tissues, but the circulating inflammatory biomarkers were not correlated with overall biomarker expression [24]. Therefore, further studies will be necessary to clarify the relationship between the tissue inflammatory cytokine or adipokine levels and EAT volume.

Finally, the present study may have been affected by selection bias, because the study was composed of patients with suspected CAD. In addition, this was a cross-sectional study with a relatively small sample size.

5. Conclusions

EAT accumulation was associated with the presence of coronary plaques with vulnerable characteristics, as detected by coronary CT angiography. A high EAT volume is a predictor of vulnerable plaque components independent of obesity measurements (BMI and VAT) and CAC scores.

Acknowledgments

The authors of this manuscript have certified that they comply with the Principles of Ethical Publishing in the International Journal of Cardiology [25].

Please cite this article as: Oka T, et al, Association between epicardial adipose tissue volume and characteristics of non-calcified plaques assessed by coronary computed tomographic angiography, Int J Cardiol (2011), doi:10.1016/j.ijcard.2011.04.021

This study was supported by the Tsuchiya Foundation, Hiroshima, Japan.

References

[1] See R, Abdullah SM, McGuire DK, et al. The association of differing measures of overweight and obesity with prevalent atherosclerosis: the Dallas Heart Study. J Am Coll Cardiol 2007;50:752–9.

[2] Yusuf S, Hawken S, Ounpuu S, et al. Obesity and the risk of myocardial infarction in 27,000 participants from 52 countries: a case-control study. Lancet 2005;366: 1640–9.

[3] Ohashi N, Yamamoto H, Horiguchi J, et al. Visceral fat accumulation as a predictor of coronary artery calcium as assessed by multislice computed tomography in Japanese patients. Atherosclerosis 2009;202:192–9.

[4] Ohashi N, Yamamoto H, Horiguchi J, et al. Association between visceral adipose tissue area and coronary plaque morphology assessed by CT angiography. JACC Cardiovasc Imaging 2010;3:908–17.

[5] Sacks HS, Fain JN. Human epicardial adipose tissue: a review. Am Heart J 2007;153:907–17.

[6] Kitagawa T, Yamamoto H, Ohhashi N, et al. Comprehensive evaluation of noncalcified coronary plaque characteristics detected using 64-slice computed tomography in patients with proven or suspected coronary artery disease. Am Heart J 2007;154:1191–8.

[7] Kitagawa T, Yamamoto H, Horiguchi J, et al. Characterization of noncalcified coronary plaques and identification of culprit lesions in patients with acute coronary syndrome by 64-slice computed tomography. JACC Cardiovasc Imaging 2009;2:153–60.

[8] Motoyama S, Sarai M, Harigaya H, et al. Computed tomographic angiography characteristics of atherosclerotic plaques subsequently resulting in acute coronary syndrome. J Am Coll Cardiol 2009;54:49–57.

[9] Djaberi R, Schuijf JD, van Werkhoven JM, Nucifora G, Jukema JW, Bax JJ. Relation of epicardial adipose tissue to coronary atherosclerosis. Am J Cardiol 2008;102: 1602–7.

[10] Sarin S, Wenger C, Marwaha A, et al. Clinical significance of epicardial fat measured using cardiac multislice computed tomography. Am J Cardiol 2008;102: 767–71.

[11] International Expert Committee. International Expert Committee report on the role of the A1C assay in the diagnosis of diabetes. Diabetes Care 2009;32:1327–34.

[12] Agatston AS, Janowitz WR, Hildner FJ, Zusmer NR, Viamonte Jr M, Detrano R. Quantification of coronary artery calcium using ultrafast computed tomography. J Am Coll Cardiol 1990;15:827–32.

[13] Konishi M, Sugiyama S, Sugamura K, et al. Association of pericardial fat accumulation rather than abdominal obesity with coronary atherosclerotic plaque formation in patients with suspected coronary artery disease. Atherosclerosis 2010;209:573–8.

[14] Nelson AJ, Worthley MI, Psaltis PJ, et al. Validation of cardiovascular magnetic resonance assessment of pericardial adipose tissue volume. J Cardiovasc Magn Reson 2009;11:15.

[15] Perseghin G, Lattuada G, De Cobelli F, et al. Increased mediastinal fat and impaired left ventricular energy metabolism in young men with newly found fatty liver. Hepatology 2008;47:51–8.

[16] Wang TD, Lee WJ, Shih FY, et al. Association of epicardial adipose tissue with coronary atherosclerosis is region-specific and independent of conventional risk factors and intra-abdominal adiposity. Atherosclerosis 2010;213:279–87.

[17] Iacobellis G, Lonn E, Lamy A, Singh N, Sharma AM. Epicardial fat thickness and coronary artery disease correlate independently of obesity. Int J Cardiol in press.

[18] Saura D, Oliva MJ, Rodriguez D, et al. Reproducibility of echocardiographic measurements of epicardial fat thickness. Int J Cardiol 2010;141:311–3.

[19] Tamarappoo B, Dey D, Shmilovich H, et al. Increased pericardial fat volume measured from noncontrast CT predicts myocardial ischemia by SPECT. JACC Cardiovasc Imaging 2010;3:1104–12.

[20] Alexopoulos N, McLean DS, Janik M, Arepalli CD, Stillman AE, Raggi P. Epicardial adipose tissue and coronary artery plaque characteristics. Atherosclerosis 2009;213:150–4.

[21] Ding J, Hsu FC, Harris TB, et al. The association of pericardial fat with incident coronary heart disease: the Multi-Ethnic Study of Atherosclerosis (MESA). Am J Clin Nutr 2009;90:499–504.

[22] Yong HS, Kim EJ, Seo HS, et al. Pericardial fat is more abundant in patients with coronary atherosclerosis and even in the non-obese patients: evaluation with cardiac CT angiography. Int J Cardiovasc Imaging 2009;26:53–62.

[23] Gorter PM, de Vos AM, van der Graaf Y, et al. Relation of epicardial and pericoronary fat to coronary atherosclerosis and coronary artery calcium in patients undergoing coronary angiography. Am J Cardiol 2008;102:380–5.

[24] Mazurek T, Zhang L, Zalewski A, et al. Human epicardial adipose tissue is a source of inflammatory mediators. Circulation 2003;108:2460–6.

[25] Shewan LG, Coats AJ. Ethics in the authorship and publishing of scientific articles Int J Cardiol 2010;144:1–2.

Please cite this article as: Oka T, et al, Association between epicardial adipose tissue volume and characteristics of non-calcified plaques assessed by coronary computed tomographic angiography, Int J Cardiol (2011), doi:10.1016/j.ijcard.2011.04.021

JACC: CARDIOVASCULAR IMAGING
© 2009 BY THE AMERICAN COLLEGE OF CARDIOLOGY FOUNDATION
PUBLISHED BY ELSEVIER INC.

VOL. 2, NO. 2, 2009
ISSN 1936-878X/09/$36.00
DOI:10.1016/j.jcmg.2008.09.015

Characterization of Noncalcified Coronary Plaques and Identification of Culprit Lesions in Patients With Acute Coronary Syndrome by 64-Slice Computed Tomography

Toshiro Kitagawa, MD,* Hideya Yamamoto, MD, FACC,* Jun Horiguchi, MD,‡ Norihiko Ohhashi, MD,* Futoshi Tadehara, MD,* Tomoki Shokawa, MD,* Yoshihiro Dohi, MD,* Eiji Kunita, MD,* Hiroto Utsunomiya, MD,* Nobuoki Kohno, MD,† Yasuki Kihara, MD, FACC*

Hiroshima, Japan

OBJECTIVES We sought to characterize noncalcified coronary atherosclerotic plaques in culprit and remote coronary atherosclerotic lesions in patients with acute coronary syndrome (ACS) with 64-slice computed tomography (CT).

BACKGROUND Lower CT density, positive remodeling, and adjacent spotty coronary calcium are characteristic vessel changes in unstable coronary plaques.

METHODS Of 147 consecutive patients who underwent contrast-enhanced 64-slice CT examination for coronary artery visualization, 101 (ACS; n = 21, non-ACS; n = 80) having 228 noncalcified coronary atherosclerotic plaques (NCPs) were studied. Each NCP detected within the vessel wall was evaluated by determining minimum CT density, vascular remodeling index (RI), and morphology of adjacent calcium deposits.

RESULTS The CT visualized more NCPs in ACS patients (65 lesions, 3.1 ± 1.2/patient) than in non-ACS patients (163 lesions, 2.0 ± 1.1/patient). Minimum CT density (24 ± 22 vs. 42 ± 29 Hounsfield units [HU], $p < 0.01$), RI (1.14 ± 0.18 vs. 1.08 ± 0.19, $p = 0.02$), and frequency of adjacent spotty calcium of NCPs (60% vs. 38%, $p < 0.01$) were significantly different between ACS and non-ACS patients. Frequency of NCPs with minimum CT density <40 HU, RI >1.05, and adjacent spotty calcium was approximately 2-fold higher in the ACS group than in the non-ACS group (43% vs. 22%, $p < 0.01$). In the ACS group, only RI was significantly different between 21 culprit and 44 nonculprit lesions (1.26 ± 0.16 vs. 1.09 ± 0.17, $p < 0.01$), and a larger RI (≥1.23) was independently related to the culprit lesions (odds ratio: 12.3; 95% confidential interval: 2.9 to 68.7, $p < 0.01$), but there was a substantial overlap of the distribution of RI values in these 2 groups of lesions.

CONCLUSIONS Sixty-four-slice CT angiography demonstrates a higher prevalence of NCPs with vulnerable characteristics in patients with ACS as compared with stable clinical presentation. (J Am Coll Cardiol Img 2009;2:153–60) © 2009 by the American College of Cardiology Foundation

From the Departments of *Cardiovascular Medicine, and †Molecular and Internal Medicine, Graduate School of Biomedical Sciences, Hiroshima University, Hiroshima, Japan; and the ‡Department of Clinical Radiology, Hiroshima University Hospital, Hiroshima, Japan.

Manuscript received August 19, 2008; revised manuscript received September 16, 2008, accepted September 24, 2008.

JACC: CARDIOVASCULAR IMAGING, VOL. 2, NO. 2, 2009
FEBRUARY 2009:153–60

The recently developed technology of multidetector computed tomography (MDCT) has the potential to noninvasively identify and characterize noncalcified coronary atherosclerotic plaques (NCPs) in vivo (1,2). A potentially interesting application would be the identification of patients or individual coronary lesions with an increased likelihood of plaque rupture or erosion, leading to acute coronary events. Some previous studies have identified plaque characteristics typically observed by computed tomography (CT) in patients with acute coronary syndrome (ACS). Such characteristics included lower CT density, positive remodeling (PR), and adjacent spotty calcium deposits (3,4). We previously reported that, in comparison with intravascular ultrasound (IVUS), 64-slice CT allows reliable analysis of the components, vascular remodeling, and adjacent calcium morphology of NCPs and could document that lower CT density, PR, and adjacent spotty coronary calcium frequently co-existed in potentially "vulnerable" lesions (5). We consequently hypothesize that these morphologic factors of NCPs might act synergistically to increase the risk of ACS.

See page 161

ABBREVIATIONS AND ACRONYMS

ACS = acute coronary syndrome
CT = computed tomography
ECG = electrocardiogram
HU = Hounsfield units
IVUS = intravascular ultrasound
MDCT = multidetector computed tomography
NCP = noncalcified coronary atherosclerotic plaque
NSTEMI = non–ST-segment elevation myocardial infarction
PR = positive remodeling
RI = remodeling index

Although most previous analyses were limited to culprit lesions in ACS patients (3,4), we designed the study reported here to characterize all NCPs—including nonculprit lesions—in patients with ACS with 64-slice CT. We also compared the NCP characteristics in patients with ACS with others with stable coronary artery disease.

METHODS

Study patients. From November 2006 to October 2007, we enrolled 147 consecutive patients with proven or suspected coronary artery disease (96 men and 51 women, 67 ± 11 years), who underwent MDCT angiography for follow-up or diagnosis of coronary artery disease. Exclusion criteria for MDCT angiography included cardiac arrhythmias (i.e., atrial fibrillation or frequent paroxysmal premature beats), contraindications for iodinated contrast medium, unstable hemodynamic conditions, and ST-segment elevation myocardial infarction. Furthermore, patients with previous ACS, percutaneous coronary intervention, and/or coronary artery bypass grafting were excluded. The study was approved by our hospital's ethical committee, and written informed consent was obtained from all patients.

We assigned patients to the ACS (non–ST-segment elevation myocardial infarction [NSTEMI] and unstable angina) or the non-ACS group according to standard criteria (6). Specifically, NSTEMI was defined as a new finding of ST-segment depression of >0.1 mm or T-wave inversion of at least 0.3 mm in more than 2 anatomically contiguous leads and elevation of troponin-I levels (>0.05 ng/ml). Unstable angina was defined as a new onset of severe, progressive, or resting angina without elevation of electrocardiographic (ECG) ST-segment and troponin-I level. Patients without any of these criteria and with stable clinical presentation (equivocal or positive cardiac stress test, atypical chest pain, or stable exertional chest pain) were assigned to the non-ACS group.

For all patients in the ACS group, invasive coronary angiography was performed within 24 h after MDCT angiography. Vessel narrowing was measured with quantitative coronary angiography analysis (QCA-CMS, Version 5.3, MEDIS Medical Imaging Systems, Leiden, the Netherlands) in the projection that revealed the highest degree of stenosis, and obstructive stenosis was defined as luminal diameter narrowing >50% compared with the reference site. Per patient, 1 single obstructive coronary stenosis was identified as the culprit lesion. When multiple obstructive coronary stenoses were detected, the culprit lesion was defined as the lesion whose appearance was associated with ECG changes or as the lesion with the most obstructive luminal narrowing.

MDCT scan protocol and reconstruction. MDCT angiography was performed with a 64-slice CT scanner (LightSpeed VCT, GE Healthcare, Waukesha, Wisconsin; gantry rotation time, 0.35 s; 64 × 0.625 mm detector collimation, retrospective ECG gating). Patients with a resting heart rate ≥60 beats/min received 40 mg metoprolol orally 60 min before MDCT scanning; all received 0.3 mg nitroglycerin sublingually just before scanning. Our scan protocol and reconstruction methods have been described previously (5). In brief, after a plain scan to determine the calcium burden of the coronary tree and measure coronary calcium score according to the standard Agatston method (sequential scan with 16 × 2.5 mm collimation; tube current 140 mA; tube voltage 120 kV), we acquired a contrast-enhanced data set 30 to 50 ml (0.6 to 0.7 ml/kg) contrast medium (Iopamidol, 370 mg I/ml, Bayer Healthcare, Berlin, Germany) during an inspiratory

breath-hold. The volume data set was acquired in helical mode (64 × 0.625 mm collimation; CT pitch factor, 0.18 to 0.24:1; tube current, 600 to 750 mA with ECG-correlated tube current modulation; tube voltage, 120 kV). The effective radiation dose was estimated on the basis of the dose-length product and ranged from 15 to 18 mSv (5). Image reconstruction was performed with image-analysis software (CardIQ, GE Healthcare) on a dedicated computer workstation (Advantage Workstation Ver.4.2, GE Healthcare). A "standard" kernel was used as the reconstruction filter. Depending on heart rate, either a half-scan (temporal window = 175 ms) or multi-segment (temporal window <175 ms) reconstruction algorithm was selected, and the optimal cardiac phase with the least motion artifacts was chosen individually.

Evaluation of NCP characteristics. All coronary segments >2 mm in diameter were evaluated by 2 blinded and independent observers with curved multiplanar reconstructions and cross-sectional images rendered perpendicular to the vessel center line. The definitions of NCPs and coronary calcium were as follows (5): NCP: a low-density mass >1 mm^2 in size, located within the vessel wall and clearly distinguishable from the contrast-enhanced coronary lumen and the surrounding pericardial tissue; coronary calcium: a structure on the vessel wall with a CT density above that of the contrast-enhanced coronary lumen or with a CT density of >120 Hounsfield units (HU) assigned to the coronary artery wall in a plain image. For NCPs and calcium analyses, the optimal image display setting was chosen on an individual basis; in general, the window was between 700 and 1,000 HU, and the level between 100 and 200 HU.

As previously described (5), we determined the minimum CT density in each NCP by placing at least 5 regions of interest (area = 1 mm^2) in each lesion and documenting the lowest average value of all regions of interest, and on the basis of our previous results (5), low-density NCPs were defined as lesions with a minimum CT density of <40 HU. We also determined the extent of luminal enhancement of each coronary lesion by placing a region of interest (area = 1 mm^2) in the center of the coronary artery lumen at the respective reference segment. On the basis of measurements of the cross-sectional vessel areas (mm^2) at each NCP site of maximum vessel area and each proximal reference site of the same coronary artery, we calculated the "Remodeling Index" (RI). Positive remodeling was defined as RI >1.05 (7). Finally, we assessed calcium deposits in or adjacent to each NCP by determining their presence or absence and their morphology. Spotty calcium was defined as follows: length of calcium burden <3/2 of vessel diameter and width <2/3 of vessel diameter (8). If the initial classification of NCP and adjacent calcium differed among the 2 independent observers, final classification was achieved by consensus.

Statistical analysis. Coronary calcium score is expressed as median value and range, and other measurements are expressed as mean ± SD. Continuous and categorical variables were compared with the Mann-Whitney test and chi-square test, respectively. Interobserver variability of measured CT densities and cross-sectional vessel areas was determined by calculating Pearson's correlation coefficient. In comparisons between ACS and non-ACS lesions and culprit and nonculprit lesions, we used only lesion specific factors, not including patient characteristics because lesions clustered in a single patient. Parameters of NCPs were tested with a receiver-operator characteristic curve to assess their reliability as prognostic variables for predicting ACS culprit lesions. Logistic regression was used to examine the associations between NCP characteristics (RI, presence of adjacent spotty calcium, NCP CT density, and reference site CT density) and ACS culprit lesions for multivariate analysis adjusted for the location of NCPs. All analyses were done with JMP 5.0.1 statistical software (SAS Institute Inc., Cary, North Carolina). A p value of <0.05 was considered statistically significant.

RESULTS

Baseline characteristics. The mean heart rate during scanning was 61 ± 10 beats/min; mean scan time for coronary CT angiography was 6.3 ± 2.1 s. No patient experienced any complication due to MDCT, and no patient was excluded from analysis due to poor image quality of the 64-slice CT.

Of the 147 patients, 46 (31%) had no NCPs as detected by 64-slice CT angiography (31 patients had no coronary atherosclerotic lesions, and 15 patients had only calcified coronary lesions), and all 46 had presented with stable symptoms. In the remaining 101 patients (69%) (21 patients with ACS [8 NSTEMI and 13 unstable anginas] and 80 of 126 patients with stable clinical presentation [non-ACS: no symptom, atypical chest pain, or stable exertional chest pain]), CT angiography allowed detection of at least 1 coronary lesion that contained noncalcified components. A total of 228 NCPs were visualized (on average, 2.2 ± 1.2/patient; range, 1 to 5 lesions/patient). Clinical

Table 1. **Patients' Characteristics**

	ACS Group (n = 21)	Non-ACS Group (n = 80)	p Value
Age (yrs)	66 ± 11	69 ± 9	NS
Male/female	17/4	61/19	NS
Hypertension	13 (62)	53 (66)	NS
Hyperlipidemia	12 (57)	37 (46)	NS
Diabetes mellitus	8 (38)	39 (49)	NS
Previous or current smoker	12 (57)	45 (56)	NS
Statin use	8 (38)	23 (29)	NS
Heart rate (beats/min)	59 ± 7	59 ± 9	NS
Body mass index (kg/m^2)	25 ± 3	24 ± 4	NS
Coronary calcium score	184 (0–1,550)	107 (0–4,656)	NS

N = 101. Coronary calcium score is expressed as median value (range). Other data are the mean value ± SD or n (%) of patients.
ACS = acute coronary syndrome.

characteristics of the 101 patients with NCPs are shown in Table 1. There were no statistically significant differences between ACS and non-ACS groups. Figure 1 shows MDCT and invasive angiographic findings in a case with ACS.

Comparisons of NCP findings between ACS and non-ACS patients. Sixty-five and 163 NCPs were detected in the ACS (n = 21) and non-ACS (n = 80) group, respectively. The location of NCPs in the ACS and non-ACS groups was similar (6% and 10% in the left main coronary artery, 37% and 39% in the left anterior descending artery, 20% and 15% in the left circumflex artery, 37% and 36% in the right coronary artery, respectively). The mean number of NCPs/patient was significantly higher in the ACS group (3.1 ± 1.2) than in the non-ACS group (2.0 ± 1.1, $p < 0.01$). Comparisons of NCP characteristics between the 2 groups are shown in Table 2. Excellent inter-observer agreement was found for minimum CT densities of NCPs ($r = 0.91$), for luminal densities at the reference site lumens ($r = 0.94$), and for all cross-sectional vessel areas ($r = 0.88$). The minimum CT density of NCPs was significantly lower in the ACS group (24 ± 22 HU) than in the non-ACS group (42 ± 29 HU, $p < 0.01$). There was no difference in mean CT densities of reference site lumens between the ACS and non-ACS groups. The mean RI of NCPs was significantly higher in the ACS group than in the non-ACS group (1.14 ± 0.18 vs. 1.08 ± 0.19, $p = 0.02$). Noncalcified coronary atherosclerotic plaques were more frequently associated with spotty calcification in the ACS group (60%) as compared with the non-ACS group (38%, $p < 0.01$). Furthermore, the frequency of low-density NCPs with PR and spotty calcium was substantially higher in the ACS group (43%) than in the non-ACS group (22%, $p < 0.01$).

CT characteristics of culprit versus nonculprit lesions in ACS patients. In the 21 ACS patients, 21 culprit and 44 nonculprit NCPs were detected. Of these lesions, 32 (21 culprit and 11 nonculprit) were assessed as obstructive (>50% stenosis) by invasive angiography. Comparisons of NCP characteristics between culprit and nonculprit lesions in the ACS group are shown in Table 3. The frequency of adjacent spotty calcium was similar in both types of plaques (57% vs. 61%). The minimum CT density of the culprit lesions tended to be lower than that of the nonculprit lesions (15 ± 13 HU vs. 28 ± 24 HU), but this difference did not reach statistical significance. The mean RI of the culprit lesions (1.26 ± 0.16) was significantly higher than that of the nonculprit lesions (1.09 ± 0.17, $p < 0.01$), but there was a substantial overlap of the distribution of RI values in these 2 groups of lesions (Fig. 2). The optimal cutoff for RI by CT angiography to predict culprit lesions was 1.23 and had a sensitivity of 71% and specificity of 82% (area under the curve 0.77). The frequency of plaques that displayed all 3 parameters of "vulnerability" (low CT density, positive remodeling, and spotty calcium) tended to be higher for culprit lesions (57%) compared with nonculprit lesions (36%). However, the difference was not significant. Multivariate analysis, which included larger RI (≥1.23), the presence of adjacent spotty calcium, the minimum NCP CT density, and the reference site CT density, revealed that a larger RI was the only significant predictor of ACS culprit lesions (odds ratio: 12.3; 95% confidence interval: 2.9 to 68.7, $p < 0.01$). Furthermore, the mean RI of the 21 culprit lesions was significantly higher than that of the 11 obstructive nonculprit lesions (1.26 ± 0.16 vs. 1.08 ± 0.16, $p < 0.01$), whereas the minimum CT densities (15 ± 13 HU vs. 15 ± 18 HU), frequencies of adjacent spotty calcium (57% vs. 64%), and frequencies of low-density NCPs with PR and spotty calcium (57% vs. 45%) were similar.

DISCUSSION

In this study, we demonstrated that 64-slice CT coronary angiography allows visualization of more noncalcified coronary atherosclerotic lesions with characteristics assumed to be associated with plaque "vulnerability" in patients with ACS as compared with patients with stable clinical presentation. Thus, 64-slice CT might contribute toward the differentiation of "vulnerable patients." Furthermore, we observed that a high degree of positive remodeling is the most

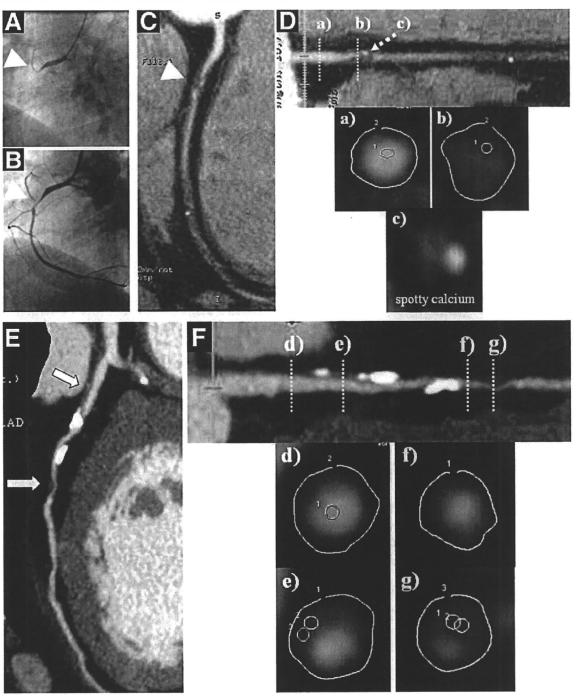

Figure 1. **Invasive Angiography and Coronary CT Angiography in a 58-Year-Old Man With NSTEMI**

(A and B) Invasive coronary angiographic images show an initial occlusion of the proximal portion of the right coronary artery (RCA) **(arrowhead)** and a recanalization of the lesion. **(C and D)** Curved multiplanar reconstruction (MPR) images show the subtotal occlusion and noncalcified coronary atherosclerotic plaque (NCP) with spotty calcium in the proximal portion of the RCA **(arrowhead)**. The cross-sectional vessel areas of the reference site **(a)** and NCP **(b)** are 23 and 29 mm^2, respectively. Therefore, the remodeling index (RI) is 1.26. The minimum computed tomography (CT) density of the NCP is 16 Hounsfield units (HU) **(b)**. Spotty calcium with the NCP is observed in the cross-sectional image **(c)**. **(E and F)** Curved MPR images show multiple nonculprit NCP in left anterior descending coronary artery (LAD) **(arrows)**. The cross-sectional vessel areas of the reference site **(d)** and nonobstructive NCP **(e)** in the proximal portion are 28 and 28 mm^2, respectively. Therefore, the RI is 1.0. The minimum CT density of the NCP is 44 HU **(e)**. The cross-sectional vessel areas of the reference site **(f)** and obstructive NCP **(g)** in the middle portion are 18 and 18 mm^2, respectively. Therefore, the RI is 1.0. The minimum CT density of the NCP is −7 HU **(g)**. NSTEMI = non–ST-segment elevation myocardial infarction.

accurate discriminator of culprit and nonculprit lesions in ACS patients. Thus, our results provide further evidence for the potential of MDCT angiography to noninvasively identify vulnerable lesions and vulnerable patients.

General findings of NCPs in ACS. In a report using 16-slice CT angiography, the prevalence of noncalcified plaque was 100% in ACS culprit lesions (3). The present study on 64-slice CT also confirms the presence of NCPs in all ACS patients and in all ACS culprit lesions, whereas no patient without any NCP had an ACS. Although the number of ACS patients was small (n = 21), this indicates a high sensitivity of NCP as detected by CT to identify patients with ACS.

Furthermore, our findings are in accordance with previous evidence that the disease process in ACS patients is not focal but more widespread throughout

Table 2. Comparison of NCP Characteristics Between ACS and Non-ACS Groups

	ACS Group (n = 65)	Non-ACS Group (n = 163)	p Value
CT density (HU)			
NCPs (minimum density)	24 ± 22	42 ± 29	< 0.01
Reference site	351 ± 44	357 ± 62	0.46
Remodeling index	1.14 ± 0.18	1.08 ± 0.19	0.02
Adjacent spotty calcium, (n [%])	39 (60)	62 (38)	< 0.01
Low-density NCPs (<40 HU) with PR and spotty calcium, (n [%])	28 (43)	36 (22)	< 0.01

Data are the mean value ± SD or n (%) of non-calcified coronary atherosclerotic plaque (NCPs).
ACS = acute coronary syndrome; CT = computed tomography; HU = Hounsfield units; PR = positive remodeling.

the coronary circulation and might lead to instability of multiple plaques (9). In fact, multiple plaque ruptures in locations other than on the culprit lesion have been detected by IVUS in patients with ACS (10). In the present study, with 64-slice CT angiography that can evaluate the entire coronary tree, more NCPs/patient were detected in the ACS group than the non-ACS group, and those that were detected more frequently displayed "vulnerable" characteristics, such as lower CT density, extent of arterial remodeling, and presence of adjacent spotty calcium. Motoyama et al. (4) reported that 47% of culprit lesions in ACS had all 3 characteristics of PR (RI >1.1), low CT density (<30 HU), and spotty calcium (<3 mm in size). We also observed that 43% of NCPs in the ACS group had all 3 vulnerable characteristics, although the criteria we used varied slightly. This indicates that multiple vulnerable plaques with characteristics similar to the culprit lesion are often present in the entire coronary tree of ACS patients.

Predictors of ACS culprit lesions in MDCT. A previous study with CT angiography (4) revealed that, among the 3 vulnerable characteristics, positive remodeling was the strongest discriminator between culprit and nonculprit lesions in patients with ACS (PR: 87%; low CT density: 79%; spotty calcium: 63%), similar to our results. Whereas this could be explained by previous data, such as a histopathological study using postmortem hearts that revealed that coronary plaques with PR had a higher lipid content and a higher macrophage count (11), or the fact that excessive expansive remodeling promotes continued local lipid accumulation, inflammation, oxidative stress, matrix breakdown, and eventually further plaque progression (12), this observation has to be interpreted with caution. In a retrospective analysis such as ours, the correlation of remodeling and culprit lesions might be a consequence of plaque rupture and not necessarily a predictor. Also, in spite of a significant difference of the mean RI between culprit and nonculprit lesions of ACS patients, the overlap of RI values in these 2 groups was substantial.

Study limitations. Caution is required when interpreting CT densities of NCPs. We cannot exclude the possibility that thrombosis might be present in some ACS culprit lesions, and low-density NCPs are indistinguishable from thromboses due to their similar densities. Thrombosis adjacent to very-low-density NCPs might increase the CT densities that were measured, and this might be 1 of the reasons that the minimum CT density is not statistically different between the culprit and nonculprit lesions in the present study. We believe that selecting the minimum density value as the NCP density is an appropriate method for limiting partial volume and beam hardening effects resulting from neighboring structures, especially hyperdense calcium. However, improvements of spatial resolution will be necessary to more reliably identify and characterize NCPs on the basis of CT densities.

Second, at present, there is no gold standard for determination of coronary plaque vulnerability in CT angiography. For example, in the previous MDCT study, spotty calcium was defined as <3 mm in size (4). However, the visual estimation of high-density structures, such as calcium deposits, varies depending on the window setting in the CT image. Therefore, we believe that our method, which is based on the comparison of calcium dimensions with vessel diameters, is more appropriate for classification of calcium deposits.

Table 3. Comparison of NCP Characteristics Between Culprit and Non-Culprit Lesions in ACS Group

	Culprit Lesions (n = 21)	Non-Culprit Lesions (n = 44)	p Value
CT density (HU)			
NCPs (minimum density)	15 ± 13	28 ± 24	0.07
Reference site	353 ± 46	350 ± 43	0.95
Remodeling index	1.26 ± 0.16	1.09 ± 0.17	< 0.01
Adjacent spotty calcium, (n [%])	12 (57)	27 (61)	0.75
Low-density NCPs (<40 HU) with PR and spotty calcium, (n [%])	12 (57)	16 (36)	0.11

Data are the mean value ± SD or n (%) of NCPs.
Abbreviations as Table 2.

Third, the present study is retrospectively designed, and we assume that vulnerable NCPs have morphological characteristics similar to those of already-disrupted NCPs—a limitation shared with previous studies in this field. A long-term, large prospective trial would be necessary to determine whether CT stratification of NCPs indeed has prognostic value for predicting future cardiac events. Future approaches might, in fact, extend beyond CT analysis of plaque morphology, such as demonstrated by a recent report that described the use of a dedicated contrast agent to visualize macrophage infiltration in atherosclerotic plaques (13).

Finally, our data acquisition protocol led to a relatively high radiation dose for coronary CT angiography. Recently, a prospectively ECG-triggered algorithm has been developed that allows imaging with substantially reduced dose (14). Further studies will be required to validate the accuracy for identification and characterization of NCPs with newer low-dose algorithms.

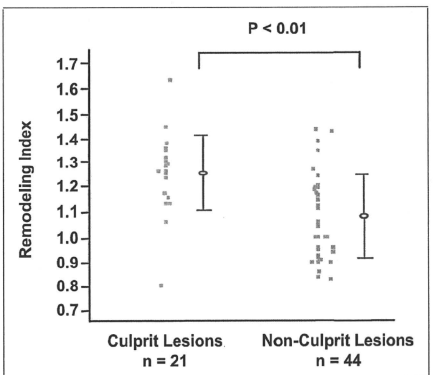

Figure 2. Comparison of RI Between ACS Culprit and Nonculprit Lesions

The mean RI of the culprit lesions is significantly higher than that of the non-culprit lesions (1.26 ± 0.16 vs. 1.09 ± 0.17, $p < 0.01$), but there is a substantial overlap of the distribution of RI values in these 2 groups of lesions. ACS = acute coronary syndrome; RI = remodeling index.

CONCLUSIONS

We were able to demonstrate that 64-slice coronary CT angiography detects a higher number of atherosclerotic lesions with noncalcified components in patients with ACS as compared with patients with stable symptoms. Identifying the actual culprit lesion in ACS patients is more difficult: among the characteristics that are assumed to be associated with plaque "vulnerability" in CT, a large degree of positive remodeling was the only independent predictor of culprit lesions in ACS patients, but a large variability was observed concerning the extent of positive remodeling in culprit and nonculprit lesions. Rather than identifying a single lesion responsible for a future coronary event, the ability to investigate plaque characteristics throughout the entire coronary system in a noninvasive fashion might be an important property of coronary CT angiography regarding its potential application in the context of identifying "vulnerable patients" at risk for ACS.

Acknowledgments

The authors are grateful to Nobuhiko Hirai, MD, and Masao Kiguchi, RT, for their technical assistance. The authors also thank Dr. Shozo Miki for his critical reading of the manuscript.

Reprint requests and correspondence: Dr. Hideya Yamamoto, Department of Cardiovascular Medicine, Graduate School of Biomedical Sciences, Hiroshima University, 1-2-3 Kasumi Minami-ku, Hiroshima 734-8551, Japan. *E-mail: hideyayama@hiroshima-u.ac.jp.*

REFERENCES

1. Hausleiter J, Meyer T, Hadamitzky M, et al. Prevalence of noncalcified coronary plaques by 64-slice computed tomography in patients with an intermediate risk for significant coronary artery disease. J Am Coll Cardiol 2006;46:312–8.
2. Butler J, Shapiro M, Reiber J, et al. Extent and distribution of coronary artery disease: A comparative study of invasive versus noninvasive angiography with computed tomography. Am Heart J 2007;153:378–84.
3. Hoffmann U, Moselewski F, Nieman K, et al. Noninvasive assessment of plaque morphology and composition in culprit and stable lesions in acute coronary syndrome and stable lesions in stable angina by multidetector computed tomography. J Am Coll Cardiol 2006;47:1655–62.
4. Motoyama S, Kondo T, Sarai M, et al. Multislice computed tomographic characteristics of coronary lesions in acute coronary syndromes. J Am Coll Cardiol 2007;50:319–26.
5. Kitagawa T, Yamamoto H, Ohhashi N, et al. Comprehensive evaluation of noncalcified coronary plaque characteristics detected using 64-slice computed tomography in patients with proven or suspected coronary artery disease. Am Heart J 2007;154:1191–8.
6. Braunwald E, Antman EM, Beasley JW, et al. ACC/AHA 2002 guideline update for the management of patients with unstable angina and non–ST-segment elevation myocardial infarction-summary article: a report of the American College of Cardiology/American Heart Association Task Force on Practice Guidelines (Committee on the Management of Patients With Unstable Angina). J Am Coll Cardiol 2002;40:1366–74.

7. Achenbach S, Ropers D, Hoffmann U, et al. Assessment of coronary remodeling in stenotic and nonstenotic coronary atherosclerotic lesions by multidetector spiral computed tomography. J Am Coll Cardiol 2004;43:842–7.
8. Kajinami K, Seki H, Takekoshi N, et al. Coronary calcification and coronary atherosclerosis: site by site comparative morphologic study of electron beam computed tomography and coronary angiography. J Am Coll Cardiol 1997;29:1549–56.
9. Buffon A, Biasucci LM, Liuzzo G, et al. Widespread coronary inflammation in unstable angina. N Eng J Med 2002;347:5–12.
10. Rioufol G, Finet G, Ginon I, et al. Multiple atherosclerotic plaque rupture in acute coronary syndrome: a three-vessel intravascular ultrasound study. Circulation 2002;106:804–8.
11. Varnava AM, Mills PG, Davies MJ. Relationship between coronary artery remodeling and plaque vulnerability. Circulation 2002;105:939–43.
12. Chatzizisis YS, Coskun AU, Jonas M, Edelman ER, Feldman CL, Stone PH. Role of endothelial shear stress in the natural history of coronary atherosclerosis and vascular remodeling: molecular, cellular, and vascular behavior. J Am Coll Cardiol 2007;49:2379–93.
13. Hyafil F, Cornily JC, Feig JE, et al. Noninvasive detection of macrophages using a nanoparticulate contrast agent for computed tomography. Nat Med 2007;13:636–41.
14. Earls JP, Berman EL, Urban BA, et al. Prospectively gated transverse coronary CT angiography versus retrospectively gated helical technique: improved image quality and reduced radiation dose. Radiology 2008;246:742–53.

Key Words: acute coronary syndrome ■ multidetector computed tomography ■ noncalcified coronary plaque.